Investigation of the Strong Brønsted Acidity in a Novel SAPO-type Molecular Sieve, DNL-6

Xiong Su,[†] Shutao Xu,[†] Peng Tian,[†] Jinzhe Li,[†] Anmin Zheng,[§] Qiang Wang,[§] Miao Yang,[†] Yingxu Wei,[†] Feng Deng,[§] and Zhongmin Liu*,[†,‡]

[†]National Engineering Laboratory for Methanol to Olefins, Dalian National Laboratory for Clean Energy, Dalian Institute of Chemical Physics, and [‡]State Key Laboratory of Catalysis, Dalian Institute of Chemical Physics, Chinese Academy of Sciences, Dalian 116023, P. R. China

[§]State Key Laboratory of Magnetic Resonance and Atomic Molecular Physics, Wuhan Center for Magnetic Resonance Institute of Physics and Mathematics, Chinese Academy of Sciences, Wuhan 430071, P. R. China

Ⓢ *Supporting Information*

ABSTRACT: By applying analysis of multiple solid-state MAS NMR spectra, the atomic coordination environment and acidity of a novel SAPO-type molecular sieve, DNL-6, are studied. ^{27}Al MQ-MAS NMR and ^{31}P–^{27}Al MQ-HETCOR NMR spectra reveal the existence of a Si–Al–Si region with $Al(OSi)_n$ ($n = 1-4$) species in the framework of DNL-6, explaining well the high concentration of single $Si(OAl)_4$ species (3 mmol/g) accommodated in the sample. ^{13}C MAS NMR of 2-^{13}C-acetone adsorption indicates that there exist two kinds of strong Brønsted acid sites in DNL-6. One of them has similar strength as those in HZSM-5 and the other is even stronger, which is unusual in SAPO-type molecular sieves. Also, a discrepancy in Brønsted acid concentration between the theoretical and ^1H NMR experimental results has been found, revealing the occurrence of a dehydoxylation process during the calcination. The origin of the extremely strong Brønsted acid sites in DNL-6 is investigated by density functional theory calculations, which suggest that the dehydoxylation process may lead to a local structure deformation and remarkably enhance the Brønsted acidity. More importantly, DNL-6 exhibits excellent catalytic activity in the synthesis of methylamines due to its stronger acidity.
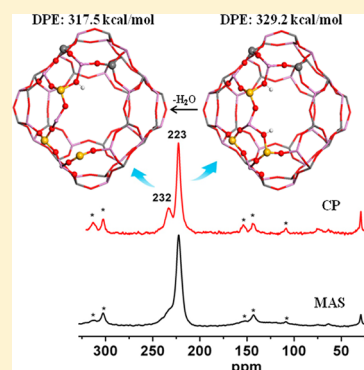
1. INTRODUCTION

Aluminophosphate (AlPO) molecular sieves and their derivatives have received considerable attention owing to their structural and compositional diversity.[1,2] Unlike aluminosilicate zeolites, the AlPO frameworks are neutral and do not exhibit intrinsic acidity. The introduction of Si atoms into the AlPO framework, resulting in the so-called SAPO materials, leads to a negatively charged framework and generates Brønsted acidity, which helps them find practical applications in adsorption and catalysis fields.[3−7] So far, many efforts have been devoted to the understanding of the correlation between acidity and framework atom arrangement of SAPO molecular sieves,[8−12] besides the extensive studies on the construction of hierarchical porosity.[13−16] It is recognized that both the Si coordination environment and Si distribution, which may vary with the structures and the Si content, have important effects on the properties of Brønsted acid sites.[9,10] The Brønsted acidity at the border of Si islands in SAPO materials is generally believed to be stronger than that of the $Si(OAl)_4$ environment.[17,18] However, up to now, all the investigated SAPO molecular sieves exhibit relatively milder acidity as compared with zeolites,[19] though a small amount of strong acid sites close to the zeolitic strength may exist, as has been identified in the acidity study of SAPO-34.[20]

DNL-6, reported by our laboratory recently, is a novel three-dimensional 8-ring SAPO molecular sieve with RHO topology possessing large *lta* cages.[21,22] Several synthesis strategies, such as CTAB-assisted hydrothermal synthesis, a phase transition method from SAPO-5 precursor, aminothermal synthesis, and hydrothermal synthesis by using SAPO dry gel as a precursor, have been successfully developed to synthesize DNL-6 molecular sieve with different Si content and coordination environments.[22−24] One interesting character of DNL-6 is that it can accommodate high concentrations of single $Si(OAl)_4$ species, which is unusual in SAPO molecular sieves and possibly relates to the large numbers of diethylamine templates confined in the *lta* cage of DNL-6. On the basis of the DNL-6 catalyst, heptamethylbenzenium cation (heptaMB$^+$), one of the most important active intermediates in the methanol to olefins (MTO) reaction, has been stabilized and captured for the first time under the real working conditions.[25] Given the high reactivity of carbenium ions, the stable existence of heptaMB$^+$ suggested the specially acidic character of DNL-6, which is not fully understood yet. We are now choosing one of the above-mentioned DNL-6 samples, which contains a high concentration of nearly single $Si(OAl)_4$ species with a Si atom fraction of 0.182 (3 mmol/g), for further acidity study.

Solid-state NMR has been demonstrated to be a well-established technique for the characterization of zeolite and related materials with respect to structure elucidation, acidity properties, and catalytic behavior.[26−28] Herein, multiple NMR experiments including one-dimensional ^{29}Si, ^{27}Al, and ^{31}P NMR; two-dimensional (2D) ^{27}Al multiple quantum magic angle spinning (MQ-MAS) NMR; and ^{31}P–^{27}Al multiple quantum heteronuclear correlation (MQ-HETCOR) NMR are carried out to study the local atomic environments in DNL-6. The acidity of DNL-6 is evaluated by ^{1}H MAS NMR and ^{13}C MAS NMR of 2-^{13}C-acetone adsorption and the temperature-programmed desorption of ammonia (NH$_3$-TPD). Density functional theory (DFT) calculations are also employed to help to understand the relationship between the local structure and the acidity. In addition, methanol amination has been employed as the probe reaction to investigate how strong the acidity of DNL-6 can affect the catalytic activity.

2. EXPERIMENTAL SECTION

2.1. Catalyst Synthesis. The synthesis procedure of DNL-6 follows a method described in our previous work.[24] In a typical synthesis, an initial gel with a molar composition of 1.0:1.0:0.3:25 Al:P:Si:H$_2$O was prepared by mixing pseudo-boehmite (70.5 wt %), water, phosphoric acid (85 wt %), and silica sol (27.5 wt %) in sequence. The mixture was stirred for 2 h and further milled for 15 min to get a homogeneous gel. Silicoaluminophosphate dry gel was obtained by the spray-drying process. Twenty grams of the resulting silicoalumino-phosphate powder was ground into powder and added into a solution consisting of 13 g of diethylamine (DEA) and 24 g of water. The final mixture was sealed into a stainless steel auto-clave and heated to 195 °C under rotation for 9 h. The ratios of the gel composition were 1.2:1.0:1.0:0.3:9.3 DEA:Al:P:Si:H$_2$O (in moles). As-synthesized products were recovered by filtra-tion, washed with deionized water, and dried at 100 °C over-night, followed by calcination at 600 °C for 3 h to remove the organic species for further characterizations.

SAPO-34 [(Al + P)/Si = 8.09] was hydrothermally syn-thesized using DEA as a template at 200 °C for 48 h. The detailed synthesis procedure has been reported in our previous work.[29] H-ZSM-5 (Si/Al = 25) was purchased as a commercial product from Tian Chuan Co.

2.2. Catalyst Characterization. Powder X-ray diffraction (PXRD) patterns were recorded on a PANalytical X'Pert PRO X-ray diffractometer equipped with Cu Kα radiation (λ = 0.154 18 nm, 40 kV, 40 mA). The chemical composition of the solid samples was determined with a Philips Magix-601 X-ray fluorescence (XRF) spectrometer. Scanning electron microscopy (SEM) images were obtained on a KYKY-AMRAY-1000B electron microscope at 20 kV.

The NH$_3$-TPD (temperature-programmed desorption) experiments were measured on an automated characterization system (Autochem 2920, Micromeritics) with a TCD detector. About 0.1 g of calcined sample was compressed into pellets (40−60 mesh) and packed into a U-tube reactor. The packed column was initially purged with a He flow and heated to 350 °C for activation. After the pretreatment, the sample was cooled to 100 °C and saturated with ammonia. Physically adsorbed ammonia was swept by purging a He flow of 40 mL min^{-1} for 30 min. Finally, the packed bed was heated at a rate of 10 °C min^{-1} to 600 °C under the He flow.

All the solid-state NMR experiments were performed on a Bruker Avance III 600 spectrometer equipped with a 14.1 tesla wide-bore magnet. The resonance frequencies were 156.4, 242.9, 119.2, and 600.13 MHz for ^{27}Al, ^{31}P, ^{29}Si, and ^{1}H, respectively. ^{27}Al and ^{31}P MAS NMR experiments were per-formed on a 4 mm MAS probe with a spinning rate of 12 kHz. ^{27}Al MAS NMR spectra were recorded using one pulse sequence, and 200 scans were accumulated with a $\pi/8$ pulse width of 0.75 μs and a 2 s recycle delay. Chemical shifts were referenced to (NH$_4$)Al(SO$_4$)$_2$·12H$_2$O at −0.4 ppm. ^{31}P MAS NMR spectra were recorded using high-power proton decoupling, and 100 scans were accumulated with a $\pi/4$ pulse width of 2.25 μs and a 4 s recycle delay. Chemical shifts were referenced to 85% H$_3$PO$_4$ at 0 ppm. ^{29}Si MAS NMR spectra were recorded with a 4 mm MAS probe with a spinning rate of 10 kHz using high-power proton decoupling, and 4096 scans were accumulated with a $\pi/4$ pulse width of 2.5 μs and a 10 s recycle delay. Chemical shifts were referenced to 4,4-dimethyl-4-silapentanesulfonate sodium salt (DSS). Before the ^{1}H MAS NMR experiment, the calcined samples were dehydrated typically at 420 °C and a pressure below 10^{-3} Pa for 20 h. ^{1}H MAS NMR spectra were recorded with a 4 mm MAS probe. The pulse width was 2.2 μs for a $\pi/4$ pulse, and 32 scans were accumulated with a 10 s recycle delay. Samples were spun at 12 kHz, and chemical shifts were referenced to adamantane at 1.74 ppm. For the determination of quantitative results, all samples were weighted, and the spectra were calibrated by mea-suring a known amount of admantane under the same conditions.

Two dimension (2D) ^{27}Al MQ-MAS and ^{27}Al−^{31}P MQ-MAS HETCOR NMR experiments were performed on a 4 mm triple-channel MAS probe at a spinning speed of 13 kHz. ^{27}Al 3Q-MAS NMR experiments were performed using a three-pulse sequence incorporating a z-filter.[30] A rf field of 83 kHz was used for the creation (0Q → ±3Q) and the first conversion (±3Q → 0Q) pulses. A rf field of 13 kHz was used for the last conversion step (0Q → ±1Q), which was the central transition selective soft 90° pulse. A two-dimensional (2D) Fourier transformation followed by a shearing transformation gave a pure absorption mode 2D contour plot.[30−32] The second-order quadrupolar effect (SOQE) and isotropic chemical shift (δ_{iso}) values were calculated according to the procedures in ref 30. The 2D ^{27}Al−^{31}P MQ-MAS HETCOR NMR spectra were acquired using the sequence similar to that in ref 33. The preliminary triple-quantum excitation and conversion in the ^{27}Al−^{31}P MQ-MAS HETCOR sequence were achieved with an rf field of 83 kHz, corresponding to pulse lengths of 5.2 and 1.7 us, respectively. The cross-polarization part of the sequence was carried out with a ^{31}P rf field of 21 kHz, an ^{27}Al rf field of 9 kHz, and a contact time of 3 ms. The spectra were acquired with 4800 scans for each of 128 experiments incrementing t_1. The recycle delay of 0.2 s resulted in a total experimental time of 34.1 h.

2-^{13}C-acetone (Cambridge Isotopes) was used to measure the acidity of the catalysts. Prior to the 2-^{13}C-acetone adsorp-tion and NMR experiments, about 0.1 g of catalyst was dehydrated at 420 °C for 15 h in a vacuum (<1 × 10^{-2} Pa). Acetone was adsorbed sufficiently on the sample at room tem-perature, and then the overloaded acetone was degassed at 40 °C for 10 min. The sample was transferred into a NMR rotor inside a glovebox under an atmosphere of nitrogen for ^{13}C MAS NMR measurement.

2.3. Theoretical Calculations. In order to accurately ob-tain the proton affinity of Brønsted acid sites inside the DNL-6 pores, one *lta* cage with AlPO composition (RHO structure)

containing 48 T atoms was taken into account by the periodic DFT calculations. During the structure optimization, the GGA-PBE functionals[34] have been considered in the spin-restricted Kohn−Sham computations with the double numerical basis set plus polarization functions (DNP) implemented in DMol3 program. The overall quality for the DMol3 calculation was set to fine, and the convergence criteria for energy, force, and displacement were 1×10^{-5} hartree, 2×10^{-3} hartree/Å, and 5×10^{-3} Å, respectively. In addition, a default fine atomic orbital cutoff (4.8 Å) and a default fine level Monkhorst−Pack k point grid ($2 \times 2 \times 2$) in the Dmol3 package were adopted.

2.4. Catalytic Reaction. The methanol amination reaction was carried out in a fixed-bed reactor at atmospheric pressure. A 1.0 g portion of the sample (40−60 mesh) was loaded into the reactor and dehydrated in He (47 mL/min) at 500 °C for 1 h prior to the reaction. The temperature of the catalyst bed was then reduced to 300 °C in He. A NH_3 flow of 25.6 mL/min was fed into the reactor by mass flow controller. Methanol was introduced into the system by passing He (47 mL/min) through a methanol-filled saturator (30 °C), which resulted in a weight-hourly space velocity (WHSV) of 1 h^{-1} and methanol/ammonia = 1 (in mole). The products were analyzed on line by an Agilent 6890 gas chromatograph with a FID detector using a CP-Volamine column.

3. RESULTS AND DISCUSSION

3.1. Atomic Coordination Environment of DNL-6. The XRD and SEM results of DNL-6 are shown in Figure S1 (Supporting Information), which demonstrate that the obtained sample possesses pure crystalline phase with RHO structure. XRF analysis reveals that the element composition of DNL-6 is $Si_{0.182}Al_{0.490}P_{0.328}O_2$.

The ^{29}Si, ^{27}Al, and ^{31}P MAS NMR spectra of DNL-6 are given in Figure 1. From ^{27}Al and ^{31}P MAS NMR spectra of calcined DNL-6, only one symmetric resonance can be observed, showing that all the T atoms of DNL-6 are tetrahedrally connected. ^{29}Si MAS NMR spectrum of as-made DNL-6 shows only one peak at −92 ppm, which can be assigned to a $Si(OAl)_4$ environment.[35] After calcination, the ^{29}Si resonance becomes broadened and there appears a minor peak at −110 ppm, which means a very small amount of siliceous islands may form in the calcined DNL-6.[36] However, the specific information about the distribution of Si atoms and the connectivity of Al and P atoms still remains unclear. The 2D MQ-MAS technique can effectively eliminate the second-order quadrupolar interaction experienced by half-integer quadrupolar nuclei and therefore narrow asymmetric line shapes considerably.[37,38] The triple quantum MAS (3Q-MAS) spectrum of DNL-6 after calcination is shown in Figure 2. The isotropic (F1) dimension displays unambiguously three peaks at 41, 48, and 53 ppm, which can be ascribed to tetrahedrally coordinated framework Al with second-order quadrupolar effect (SOQE) values of 2.8, 5.1, and 6.2 MHz and isotropic chemical shifts of 40, 44 and 47, respectively. Theoretical calculations have demonstrated that the SOQE values and chemical shifts will increase with the introduction of Si atoms.[39] Therefore, the three tetrahedrally coordinated Al species are preliminarily attributed to Al-$(OSi)_n(OP)_{(4-n)}$ ($n = 0, 1$), $Al(OSi)_n(OP)_{(4-n)}$ ($n = 2, 3$), and $Al(OSi)_4$, respectively. To confirm the assignments and obtain the information on the connectivity between P and Al atoms, HETCOR technique via a dipolar interaction can be considered.[33] Only those phosphorus nuclei that are in close proximity to aluminum nucleus can be detected in $^{27}Al-^{31}P$
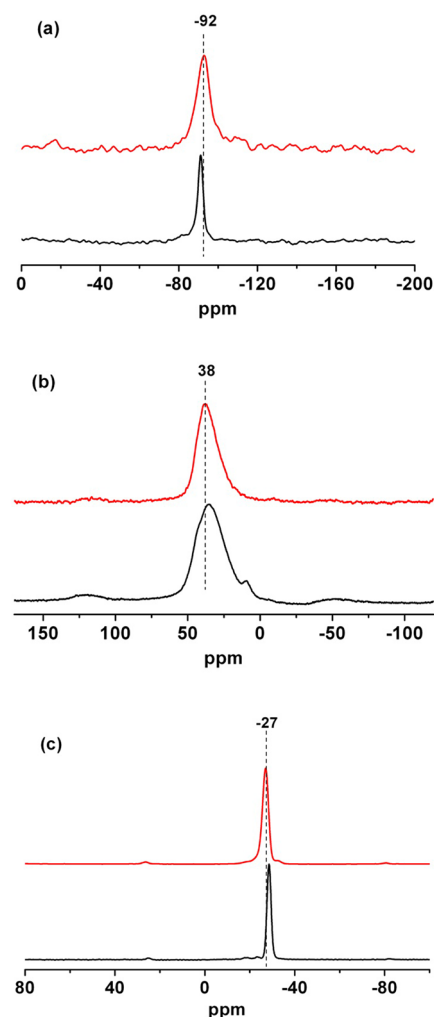

Figure 1. ^{29}Si MAS NMR (a), ^{27}Al MAS NMR (b), and ^{31}P MAS NMR (c) spectra of the DNL-6 sample. The bottom spectra are as-made DNL-6 and the top ones are calcined sample.

HETCOR experiments. Considering that standard HETCOR spectra are poorly resolved in the quadrupolar dimension because the second-order quadrupolar interaction is not fully averaged out by MAS, $^{31}P-^{27}Al$ HETCOR experiments based on MQ-MAS (Figure 2) have been employed here to generate the correlation spectra that are isotropic in both dimensions.[40] Two distinct resonances at 41 and 48 ppm corresponding to tetrahedral Al atoms can be distinguished in the ^{27}Al projection, both of which correlate to −27 ppm of the ^{31}P projection. However, the resonance at 53 ppm disappears in the ^{27}Al projection, which indicates that this Al species is not connected with P atoms. Combined with the ^{27}Al MQ-MAS NMR result, it should be assigned to Si−Al−Si regions with pure $Al(OSi)_4$ species in the framework. From the above discussions, a schematic representation containing different Si distributions in DNL-6 is depicted in Figure 3.

3.2. Acidity Study. ^1H MAS NMR is a useful and direct method to provide quantitative information on the hydroxyl protons on solid catalysts. As shown in Figure S2 (Supporting Information), the ^1H MAS NMR spectrum of the calcined DNL-6 is dominated by a signal at 3.7 ppm, which is characteristic of Brønsted acidic bridging hydroxyl groups [Si(OH)Al]. The concentration of Brønsted acidic sites is quantitatively determined by ^1H NMR as 1.99 mmol g^{-1}. However, this value
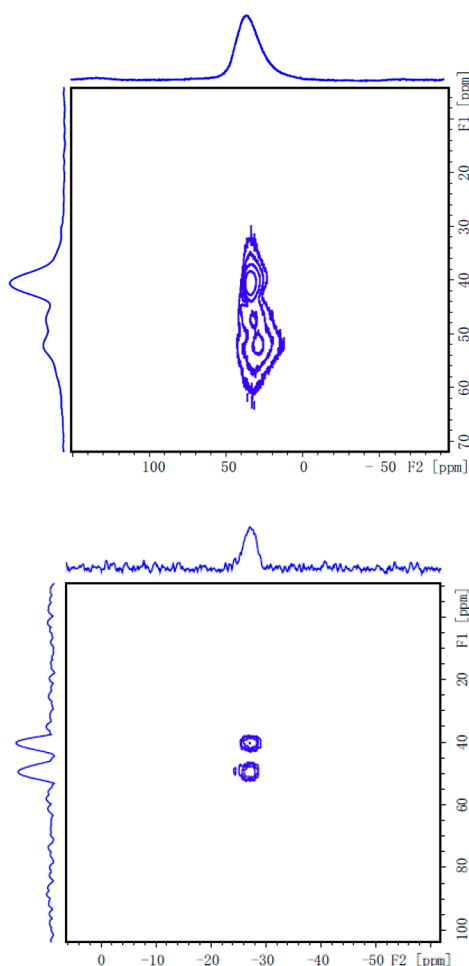
Figure 2. ^{27}Al MQ-MAS NMR spectrum (top) and $^{27}Al-^{31}P$ MQ-MAS HETCOR NMR spectrum (bottom) of the calcined DNL-6 sample.
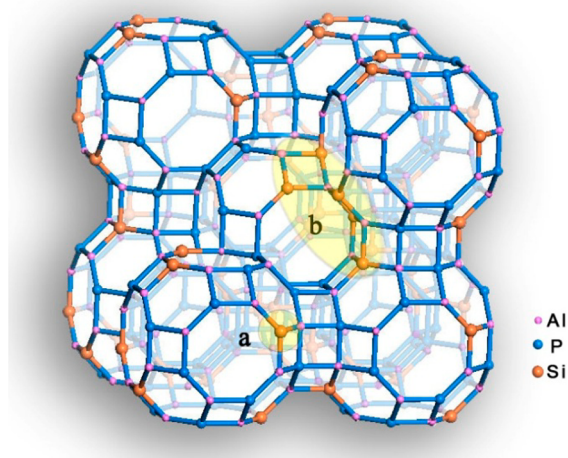

Figure 3. Schematic representation of the framework atom connectivity of DNL-6: a denotes isolated $Si(OAl)_4$ species and b denotes $Al(OSi)_4$ species.

is lower than expected on the basis of Si content in DNL-6, from which a theoretical value of 3 mmol g^{-1} is calculated, since nearly all the Si atoms exist as $Si(OAl)_4$ species and each one could generate a bridging hydroxyl group. The experimental

result only reaches 66% of its theoretical value. Such a discrepancy has not been reported before for SAPO molecular sieves. Considering the high concentration of $Si(OAl)_4$ species and their close proximity (Si−Al domains), it is speculated that a dehydroxylation process may occur during the calcination, reducing the Brønsted acid concentration, as observed in aluminosilicate zeolites.[41] Compared with the studies of Buchholz et al. and Su et al.,[36,42] the initial temperature of dehydroxylation for DNL-6 is higher than for SAPO-34, SAPO-18, and SAPO-37, which are at ca. 600 °C. The difference is possibly due to the much higher concentration of $Si(OAl)_4$ groups and their closer proximity (Si−Al domains) in DNL-6.

The acid strength of DNL-6 has been investigated by NH_3-TPD (Figure 4). For comparison, two other acidic zeolites,
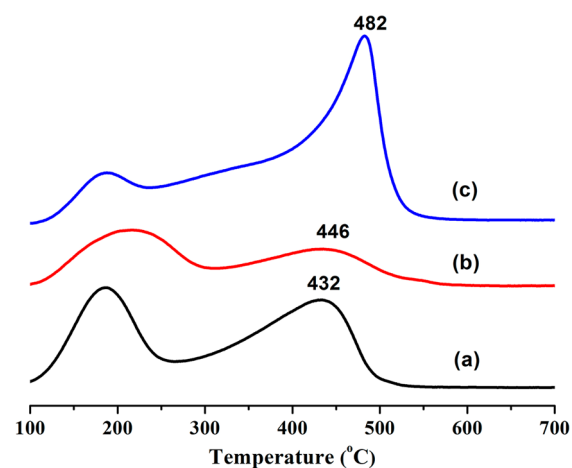

Figure 4. NH_3-TPD profiles of the samples: (a) HSAPO-34, (b) HZSM-5, and (c) DNL-6.

HZSM-5 (Si/Al = 25) and HSAPO-34 [(P + Al)/Si = 8.09], have also been tested (Figure 4). The structural characterizations of these two samples by ^{29}Si, ^{27}Al, ^{31}P, and ^1H MAS NMR spectra are shown in Figures S3 and S4 (Supporting Information). Surprisingly, DNL-6 possesses the largest acid concentration and the highest acid strength among the three samples. The position of a high-temperature desorption peak on DNL-6 is located at 482 °C, which is even higher than that on HZSM-5 (one of the most acidic zeolites), suggesting the extremely strong acidity of DNL-6. Given that the desorption temperature of NH_3 may be influenced by the small pore sizes of molecular sieves, causing misleading conclusions, solid-state ^{13}C MAS NMR of the adsorbed 2-^{13}C-acetone probe molecule, a widely used method for characterizing the acid strength of solid catalysts, was further used to examine the difference in acidity of the three samples. Generally, the adsorption of acetone on Brønsted acid sites results in the formation of a hydrogen bond between the carbonyl oxygen and acidic proton, which would induce a downfield shift of the ^{13}C NMR signal of carbonyl carbon, depending on the Brønsted acidic strength.[43,44] Figure 5 shows the ^{13}C MAS NMR spectra of samples recorded after adsorption of acetone. For HZSM-5 and HSAPO-34, sharp resonances at 224 and 214 ppm are observed respectively, suggesting the strong Brønsted acidity of ZSM-5 and the moderate acidity of HSAPO-34. Moreover, one weak signal at 225 ppm could also be observed for SAPO-34, which suggests the existence of a small amount of strong Brønsted acid sites in SAPO-34.[20] The resonance signals appearing
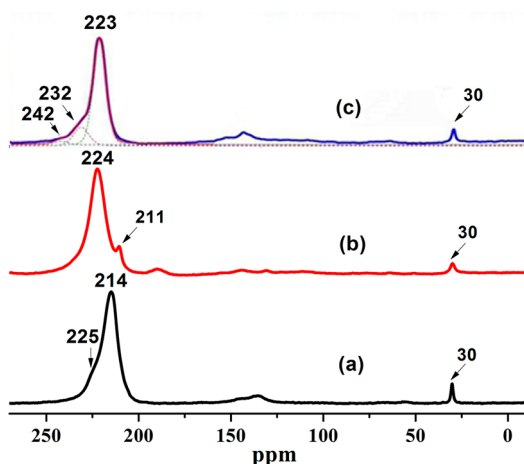
Figure 5. ^{13}C MAS NMR spectra of 2-^{13}C-acetone adsorbed in various samples: (a) HSAPO-34, (b) HZSM-5, and (c) DNL-6.

Table 1. Chemical Shifts of 2-^{13}C-Acetone Adsorbed on the Brønsted Acid Sites of Various Zeolites

sample	$\delta^{13}C$ (ppm)	ref
CDCl$_3$[a]	205	46
DNL-6	223, 232	this work
HSAPO-34	214, 225	this work
HZSM-5	224	this work
HZSM-5	223.6	46
HSAPO-34	217	46
HMOR	221.8	46
HZSM-22	225.4	46

[a]2-^{13}C-acetone dissolved in CDCl$_3$.

Scheme 1. Schematic Representation of the Dehydroxylation Process in Calcined DNL-6
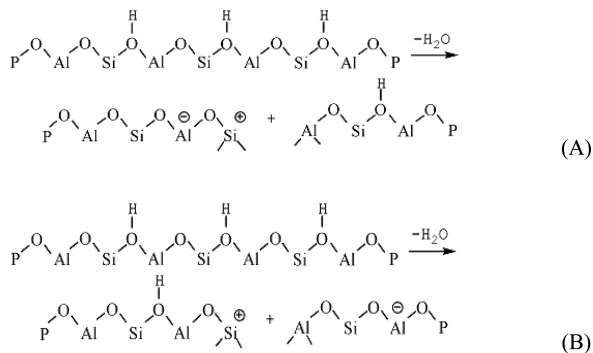
upfield, such as those at 211 and 30 ppm, are due to the reaction products of acetone adsorbed on Brønsted acid sites.[45] A dominant resonance at 223 ppm can be observed in the ^{13}C NMR of DNL-6, indicating its strong Brønsted acidity comparable to that of ZSM-5. In addition, there are two shoulder peaks at 232 and 242 ppm, respectively. The latter signal is likely associated with the acetone adsorbed on the Lewis acidic sites. Considering that no extra-framework aluminum species was observed in DNL-6, it is supposed that this site may come from the dehydroxylation process, as revealed by ^{1}H NMR. The assignment of the peak at 232 ppm is not straightforward because both Lewis acid sites and strong Brønsted acid sites may induce its appearance.[46] The [1]H−^{13}C CP/MAS NMR spectrum of acetone adsorbed on DNL-6 was
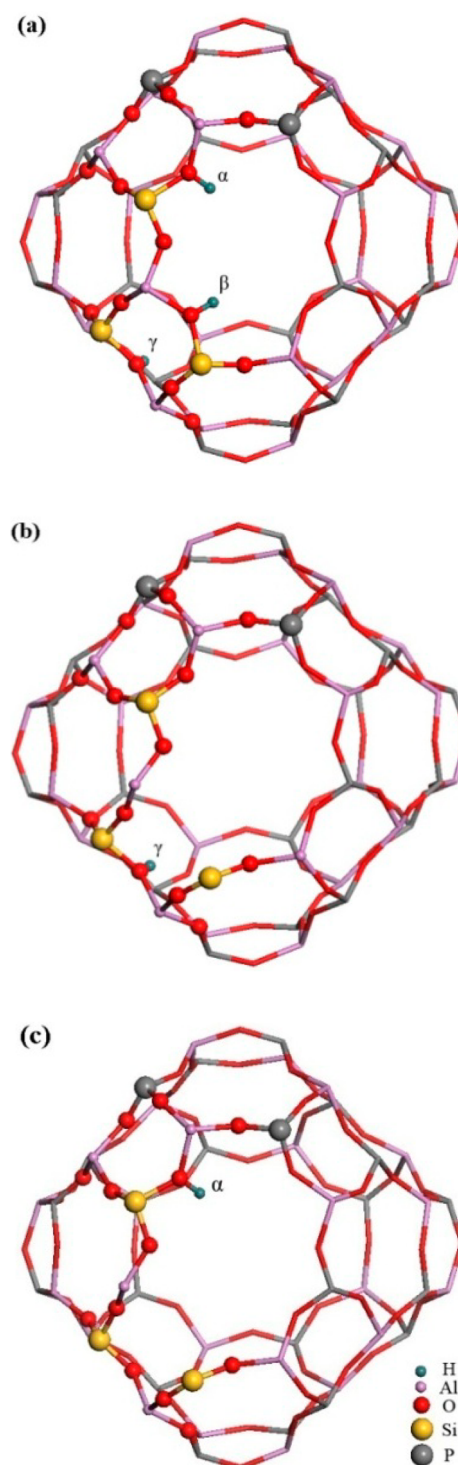

Figure 6. Optimized geometries of three adjacent Brønsted acid sites in an Al(OSi)$_3$ environment in the DNL-6 molecular sieve (a) and the corresponding dehydroxylated structures (b and c). The geometries given in parts a, b, and c are defined as island-1, island-1-H$_2$O(A), and island-1-H$_2$O(B) respectively. A and B in island-1-H$_2$O(A) and island-1-H$_2$O(B) stand for the different dehydroxylation paths shown in Scheme 1.

thus measured and is given in Figure S5 (Supporting Information). An obvious enhancement in the signal intensity at 232 ppm can be observed after cross-polarization, implying the Brønsted acid character of this signal and its strong strength. Therefore, it seems more reasonable to ascribe the

Table 2. Calculated Deprotonation Energy (DPE) of the Brønsted Acid Sites before and after Dehydration in DNL-6

calcd model	DPE value[a] (kcal mol^{-1})	calcd model	DPE value (kcal mol^{-1})	acidity enhancement
island-1	329.2	island-1-H$_2$O(A)	317.5	strong
		island-1-H$_2$O(B)	317.6	strong
island-3	328.5	island-3-H$_2$O(A)	332.1	no
		island-3-H$_2$O(B)	315.3	strong
island-2	328.6	island-1-H$_2$O(B)	330.7	no
island-4	329.4	island-4-H$_2$O(B)	314.9	strong
line-1	324.4	line-1-H$_2$O(B)	321.8	weak
line-2	324.5	line-2-H$_2$O(B)	316.8	medium
cross-1	325.2	cross-1-H$_2$O(B)	317.9	medium
cross-2	325.3	cross-2-H$_2$O(B)	318.8	medium

[a]DPE = $E_{H}^{+} + E_{ZEO}^{-} - E_{H\text{-}ZEO}$; the smaller the DPE value, the stronger the acid site.

signal at 232 ppm to acetone adsorbed on Brønsted acid sites with stronger acidity.

Table 1 compares the chemical shifts (δ_{13C}) of 2-^{13}C-acetone adsorbed on the Brønsted acid sites of various zeolites. Clearly, the values of DNL-6 are similar or higher than those of HZSM-5, HMOR, and HZSM-22, suggesting the strong Brønsted acidity of DNL-6.

3.3. Origin of the Strong Brønsted Acidity and Theoretical Calculations. The strong Brønsted acid sites in DNL-6 are unusual, and their origin deeply deserves discussion. Here, we pay more attention to the generation of the stronger Brønsted acid sites, because the acid sites corresponding to the peak at 223 ppm in the ^{13}C spectra should be mainly related to the intrinsic structure of DNL-6. According to the literature,[17,18,20,47] nonequivalent crystallographic positions of oxygen atoms and the existence of Si islands are the two commonly proposed reasons for the generation of stronger acidity in SAPO molecular sieves. The latter is obviously not the case for DNL-6 studied here, because nearly all the Si atoms exist as Si(OAl)$_4$ species. DFT calculations are thus performed to investigate the deprotonation energy (DPE) of the two nonequivalent oxygen atoms located at the intersection positions of (4, 6, 8) and (4, 4, 8) rings in the RHO framework (Figure S6, Supporting Information). A periodic *lta* cage containing 48 T atoms with AlPO$_4$ composition (one P atom replaced by Si atom) was employed as the initial model. Figure S7 (Supporting Information) presents the optimized geometry. The DPE values, defined as the energy difference between the protonated and corresponding deprotonated models, are calculated to be 323.8 and 324.3 kcal mol^{-1} for the acidic protons associated with O1 and O2 sites, respectively. The similar values obtained suggest that different oxygen sites may not be considered as the reasons for the generation of stronger Brønsted acid sites in DNL-6.

Another plausible explanation is that the dehydroxylation process that occurred among the Brønsted acid sites with close proximity during the calcination may give rise to a local structure deformation and enhance the acidity of the corresponding Brønsted acid sites. To verify this hypothesis, we use a DFT calculation method to discriminate the Brønsted acid strength before and after dehydroxylation. A periodic *lta* cage with AlPO$_4$ composition, in which three adjacent P atoms were replaced by Si atoms, was selected to represent the RHO structure. Note that there exist several possible arrangements of three Si atoms in the framework, such as Al(OSi)$_3$ and Si−Al−Si−Al−Si connection confined in one 8-ring or not. Moreover, the variable location (O1 or O2 sites) of protons together with flexible dehydroxlation paths [Schemes 1 and S1 (Supporting Information)] would create a large number of structural configurations for the theoretical calculations. Therefore, several configurations following the dehydroxlation paths shown in Scheme 1 are chosen as the representative models for calculations.

Figure 6a shows an optimized geometry of the Brønsted acid sites in an Al(OSi)$_3$ environment. The corresponding structural changes after dehydroxylation are presented in Figure 6b,c. It can be seen that only one hydroxyl proton is left associated with slight structural deformation and the cleaving of one Si−O−Al bond due to the dehydroxylation. More optimized structures of the Brønsted acid sites in DNL-6 before and after dehydroxylation are given in Figures S8 and S9 (Supporting Information). The DPE values in each configuration are theoretically determined and listed in Table 2. Upon dehydroxylation, 6.5−14.5 kcal mol^{-1} reduction of the DPE values can be observed for most of the investigated configurations, indicating that the acidity of the Brønsted acid site could be remarkably enhanced after dehydroxylation. These results support our speculation well.

From the above discussions, it is supposed that the present finding on the enhancement of Brønsted acidity may not be a unique phenomenon, because the dehydroxylation process during calcination could occur in many zeolites, especially for the zeolites with high hydroxyl group concentration. During the acidity study of zeolites, the possible microstructure changes resulting from the dehydroxylation process besides the influence of extra-framework alumina should be considered.

3.4. Catalytic Performance. Methanol amination, an acid-catalyzed reaction, is employed to test the catalytic property of DNL-6. Methylamines are important intermediates in the synthesis of fine and specialty chemicals. The commercial process for the synthesis of methylamines is operated in a high-pressure fixed bed using amorphous aluminosilicate as catalyst at temperatures of 400−430 °C. In recent years, zeolites having pore system constructed by 8-membered rings have attracted great attention as a shape-selective catalyst for this reaction.[48]

Table 3 displays the steady-state catalytic results of DNL-6. The small-pore molecular sieve HSAPO-34 [(P + Al)/Si = 8.09]

Table 3. Steady-State Conversion and Product Selectivity in the Methanol Aminiation over DNL-6 and HSAPO-34[a]

catalyst	acid concn		MeOH conv (%)	TOF (h^{-1})[d]	yield (mol %)[e]			
	A[b] (mmol/g)	B[c] (%)			MMA	DMA	TMA	CH$_4$
DNL-6	1.99	100	63.61	9.99	20.27	17.05	25.47	0.82
HSAPO-34	1.28	56	21.13	5.16	13.30	5.00	1.73	1.09

[a]Reaction conditions: 300 °C, WHSV = 1 h^{-1}, NH$_3$/CH$_3$OH = 1.0, TOS = 136 min. [b]Brønsted acid concentration determined by ^{1}H MAS NMR. [c]Medium-strong acid concentration determined by NH$_3$-TPD. The value of DNL-6 is defined as 100%. [d]TOF refers to turnover frequency, which is defined as the moles of consumed methanol per mole of Brønsted acid site per hour. [e]MMA, DMA, and TMA refer to monomethylamine, dimethylamine, and trimethylamine, respectively. Dimethyl ether is considered as a methanol resource.

was also tested in the reaction as a comparison. DNL-6 gives a methanol conversion of 63.61%, which is about 3 times higher than that of HSAPO-34 (21.13%). According to the work of Hong and co-workers,[48] Brønsted acidity in zeolites rather than Lewis acidity dictates the methylamines' synthesis; zeolites with three-dimensional structure and cage volume larger than that of *lev* cage would not exert spatial constraints for the diffusion of methylamine products. Considering that both *cha* and *lta* cages are larger than the *lev* cage, it is thus inferred that the high conversion over DNL-6 should result from its stronger Brønsted acidity. A more convincing comparison based on the turnover frequency (TOF) of methanol conversion over the Brønsted acid sites is shown in Table 1, which gives 9.99 h^{-1} for DNL-6 and 5.16 h^{-1} for HSAPO-34. In addition, the yields of three methylamine products, MMA, DMA, and TMA, over DNL-6 are also obviously higher than on HSAPO-34, though the latter shows better selectivity to MMA and DMA.

4. CONCLUSIONS

In summary, the distribution of Si atoms and the acid strength of DNL-6 have been studied amply by 1D and 2D NMR combined with theoretical calculations. It is found that the framework of DNL-6 contains Si−Al−Si regions with pure Al(OSi)$_4$ species, which explains well the high concentration of single Si(OAl)$_4$ species accommodated in the material. The Brønsted acid concentration in DNL-6, determined by ^{1}H NMR, only reaches 66% of the theoretical value. This discrepancy, rarely noticed in SAPO molecular sieves, is attributed to a dehydroxylation process during calculation, resulting from the close proximity of Si(OAl)$_4$ species. ^{13}C MAS NMR spectra of the adsorbed 2-^{13}C-acetone probe molecule reveal that DNL-6 possesses two kinds of strong Brønsted acidic sites. The former corresponds to the acid strength of HZSM-5, and the latter is even stronger. DFT theoretical calculations demonstrate that a dehydroxylation process that occurred among the Brønsted acid sites with close proximity during the calcination may result in the enhancement of Brønsted acidity. DNL-6 was used as catalyst for the methanol amination reaction and behaved with excellent catalytic activity.

■ ASSOCIATED CONTENT

ⓈSupporting Information

Details of the catalyst's characterization, NMR spectroscopy, and computational results. This material is available free of charge via the Internet at http://pubs.acs.org.

■ AUTHOR INFORMATION

Corresponding Author

* E-mail: liuzm@dicp.ac.cn. Tel: +86 41184379335.

Author Contributions

X.S. and S.X. contributed equally.

Notes

The authors declare no competing financial interest.

■ ACKNOWLEDGMENTS

■ REFERENCES

(1) Yu, J. H.; Xu, R. R. Rich Structure Chemistry in the Aluminophosphate Family. *Acc. Chem. Res.* **2003**, *36*, 481−490.

(2) Yu, J. H.; Xu, R. R. Insight into the Construction of Open-Framework Aluminophosphates. *Chem. Soc. Rev.* **2006**, *35*, 593−604.

(3) Corma, A. Inorganic Solid Acids and Their Use in Acid-Catalyzed Hydrocarbon Reactions. *Chem. Rev.* **1995**, *95*, 559−614.

(4) Corma, A.; Garcia, H. Crossing the Borders Between Homogeneous and Heterogeneous Catalysis: Developing Recoverable and Reusable Catalytic Systems. *Top. Catal.* **2008**, *48*, 8−31.

(5) Somorjai, G. A. The 13th International Symposium on Relations Between Homogeneous and Heterogeneous Catalysis—An Introduction. *Top. Catal.* **2008**, *48*, 1−7.

(6) Smit, B.; Maesen, T. L. M. Towards a Molecular Understanding of Shape Selectivity. *Nature* **2008**, *451*, 671−678.

(7) Choi, S.; Drese, J. H.; Jones, C. W. Adsorbent Materials for Carbon Dioxide Capture from Large Anthropogenic Point Sources. *ChemSusChem* **2009**, *2*, 796−854.

(8) Hasha, D.; de Saldarriaga, L. S.; Saldarriaga, C.; Hathaway, P. E.; Cox, D. F.; Davis, M. E. Studies of Silicoaluminophosphates with the Sodalite Structure. *J. Am. Chem. Soc.* **1988**, *110*, 2127−2135.

(9) Barthomeuf, D. Topological Model for The Compared Acidity of SAPOs and SiAl Zeolites. *Zeolites* **1994**, *14*, 394−401.

(10) Barthomeuf, D. Zeolites as Adsorbents and Catalysts. The Interactive System Encaged Molecule/Zeolite Framework. *Stud. Surf. Sci. Catal.* **1997**, *105*, 1677−1706.

(11) Sastre, G.; Lewis, D. W.; Catlow, C. R. A. Structure and Stability of Silica Species in SAPO Molecular Sieves. *J. Phys. Chem.* **1996**, *100*, 6722−6730.

(12) Sastre, G.; Lewis, D. W.; Catlow, C. R. A. Mechanisms of Silicon Incorporation in Aluminophosphate Molecular Sieves. *J. Mol. Catal. A: Chem.* **1997**, *119*, 349−356.

(13) Yang, X. Y.; Vantomme, A.; Lemaire, A.; Xiao, F. S.; Su, B. L. A Highly Ordered Mesoporous Aluminosilicate, CMI-10, with a Si/Al Ratio of One. *Adv. Mater.* **2006**, *18*, 2117−2122.

(14) Chen, L. H.; Li, X. Y.; Tian, G.; Li, Y.; Tan, H. Y.; Van Tendeloo, G.; Zhu, G. S.; Qiu, S. L.; Yang, X. Y.; Su, B. L. Multimodal Zeolite-Beta-Based Catalysts with a Hierarchical, Three-Level Pore Structure. *ChemSusChem* **2011**, *4*, 1452−1456.

(15) Yang, X. Y.; Léonard, A.; Lemaire, A.; Tian, G.; Su, B. L. Self-Formation Phenomenon to Hierarchically Structured Porous Materials: Design, Synthesis, Formation Mechanism and Applications. *Chem. Commun.* **2011**, *47*, 2763−2786.

(16) Yang, X. Y.; Tian, G.; Chen, L. H.; Li, Y.; Rooke, J. C.; Wei, Y. X.; Liu, Z. M.; Deng, Z.; Van Tendeloo, G.; Su, B. L. Well-Organized Zeolite Nanocrystal Aggregates with Interconnected Hierarchically Micro−Meso−Macropore Systems Showing Enhanced Catalytic Performance. *Chem.—Eur. J.* **2011**, *17*, 14987−14995.

(17) Catlow, C. R. A.; Bell, R. G.; Gale, J. D. Computer Modeling as a Technique in Materials Chemistry. *J. Mater. Chem.* **1994**, *4*, 781−792.

(18) Sastre, G.; Lewis, D. W. Modelling of Brønsted Acidity in AFI and CHA Zeotypes. *J. Chem. Soc., Faraday Trans.* **1998**, *94*, 3049−3058.

(19) Katada, N.; Nouno, K.; Lee, J. K.; Shin, J.; Hong, S. B.; Niwa, M. Acidic Properties of Cage-Based, Small-Pore Zeolites with Different Framework Topologies and Their Silicoaluminophosphate Analogues. *J. Phys. Chem. C* **2011**, *115*, 22505−22513.

(20) Shen, W. L.; Li, X.; Wei, Y. X.; Tian, P.; Deng, F.; Han, X. W.; Bao, X. H. A Study of the Acidity of SAPO-34 by Solid-State NMR Spectroscopy. *Microporous Mesoporous Mater.* **2012**, *158*, 19−25.

(21) Tian, P.; Su, X.; Wang, Y. X.; Xia, Q. H.; Zhang, Y.; Fan, D.; Meng, S. H.; Liu, Z. M. Phase-Transformation Synthesis of SAPO-34 and a Novel SAPO Molecular Sieve with RHO Framework Type from a SAPO-5 precursor. *Chem. Mater.* **2011**, *23*, 1406−1413.

(22) Su, X.; Tian, P.; Li, J. Z.; Zhang, Y.; Meng, S. H.; He, Y. L.; Fan, D.; Liu, Z. M. Synthesis and Characterization of DNL-6, a New Silicoaluminophosphate Molecular Sieve with The RHO Framework. *Microporous Mesoporous Mater.* **2011**, *144*, 113−119.

(23) Fan, D.; Tian, P.; Xu, S. T.; Xia, Q. H.; Su, X.; Zhang, L.; Zhang, Y.; He, Y. L.; Liu, Z. M. A Novel Solvothermal Approach To

Synthesize SAPO Molecular Sieves Using Organic Amines as the Solvent and Template. *J. Mater. Chem.* **2012**, *22*, 6568−6574.

(24) Su, X.; Tian, P.; Fan, D.; Xia, Q. H.; Yang, Y.; Xu, S. T.; Zhang, L.; Zhang, Y.; Wang, D. H.; Liu, Z. M. Synthesis of DNL-6 with a High Concentration of Si(4Al) Environments and its Application in CO_2 Separation. *ChemSusChem* **2013**, *6*, 911−918.

(25) Li, J. Z.; Wei, Y. X.; Chen, J. R.; Tian, P.; Su, X.; Xu, S. T.; Qi, Y.; Wang, Q. Y.; Zhou, Y.; He, Y. L.; Liu, Z. M. Observation of Heptamethylbenzenium Cation over SAPO-type Molecular Sieve DNL-6 under Real MTO Conversion Conditions. *J. Am. Chem. Soc.* **2012**, *134*, 836−839.

(26) Fyfe, C. A.; Thomas, J. M.; Klinowski, J.; Gobbi, G. C. Magic-Angle-Spinning NMR (MAS-NMR) Spectroscopy and the Structure of Zeolites. *Angew. Chem., Int. Ed.* **1983**, *22*, 259−275.

(27) Zhang, W. P.; Xu, S. T.; Han, X. W.; Bao, X. H. In Situ Solid-State NMR For Heterogeneous Catalysis: A Joint Experimental and Theoretical Approach. *Chem. Soc. Rev.* **2012**, *41*, 192−210.

(28) Xu, S. T.; Zheng, A. M.; Wei, Y. X.; Chen, J. R.; Li, J. Z.; Chu, Y. Y.; Zhang, M. Z.; Wang, Q. Y.; Zhou, Y.; Wang, J. B.; Deng, F.; Liu, Z. M. Direct Observation of Cyclic Carbenium Ions and Their Role in the Catalytic Cycle of the Methanol-to-Olefin Reaction over Chabazite Zeolites. *Angew. Chem., Int. Ed.* **2013**, *52*, 11564−11568.

(29) Liu, G. Y.; Tian, P.; Li, J. Z.; Zhang, D. Z.; Zhou, F.; Liu, Z. M. Synthesis, Characterization and Catalytic Properties of SAPO-34 Synthesized Using Diethylamine as a Template. *Microporous Mesoporous Mater.* **2008**, *1−3*, 143−149.

(30) Smith, M. E.; van Eck, E. R. H. Recent Advances in Experimental Solid State NMR Methodology for Half-Integer Spin Quadrupolar Nuclei. *Prog. Nucl. Magn. Reson. Spectrosc.* **1999**, *34*, 159−201.

(31) Rocha, J.; Morais, C. M.; Fernandez, C. Progress in Multiple-Quantum Magic-Angle Spinning NMR Spectroscopy. *Top. Curr. Chem.* **2004**, *246*, 141.

(32) Medek, A.; Harwood, J. S.; Frydman, L. Multiple-Quantum Magic-Angle Spinning NMR: A New Method for The Study of Quadrupolar Nuclei in Solids. *J. Am. Chem. Soc.* **1995**, *117*, 12779−12787.

(33) Fernandez, C.; Morais, C.; Rocha, J.; Pruski, M. High-resolution Heteronuclear Correlation Spectra between P-31 and Al-27 in Microporous Aluminophosphates. *Solid State Nucl. Magn. Reson.* **2002**, *21*, 61−70.

(34) Perdew, J. P. Generalized Gradient Approximations for Exchange and Coorrelation—A Look Backward and Forward. *Physica B* **1991**, *172*, 1−6.

(35) Vomscheid, R.; Briend, M.; Peltre, M. J.; Man, P. P.; Barthomeuf, D. The Role of the Template in Directing the Si Distribution in SAPO Zeolites. *J. Phys. Chem.* **1994**, *98*, 9614−9618.

(36) Buchholz, A.; Wang, W.; Xu, M.; Arnold, A.; Hunger, M. Thermal Stability and Dehydroxylation of Brønsted Acid Sites in Silicoaluminophosphates H-SAPO-11, H-SAPO-18, H-SAPO-31, and H-SAPO-34 Investigated by Multi-Nuclear Solid-State NMR Spectroscopy. *Microporous Mesoporous Mater.* **2002**, *56*, 267−278.

(37) Frydman, L.; Harwood, J. S. Isotropic Spectra of Half-Integer Quadrupolar Spins from Bidimensional Magic-Angle-Spinning NMR. *J. Am. Chem. Soc.* **1995**, *117*, 5367−5368.

(38) Fernandez, C.; Amoureux, J. P. 2D Multiquantum MAS-NMR Spectroscopy of Al-27 in Aluminophosphate Molecular-Sieves. *Chem. Phys. Lett.* **1995**, *242*, 449−454.

(39) Koller, H.; Meiljer, E. L.; van Santen, R. A. Al-27 Quadrupole Interaction in Zeolites Loaded with Probe Molecules—A Quantum-Chemical Study of Trends in Electric Field Gradients and Chemical Bonds in Clusters. *Solid State Nucl. Magn. Reson.* **1997**, *9*, 165−175.

(40) Wang, S. H.; De Paul, S. M.; Bull, L. M. High-Resolution Heteronuclear Correlation between Quadrupolar and Spin-1/2 Nuclei Using Multiple-Quantum Magic-Angle Spinning. *J. Magn. Reson.* **1997**, *125*, 364−368.

(41) Sonoemans, M. H. W.; den Heijer, C.; Crocker, M. Studies on the Acidity of Mordenite and ZSM-5. 2. Loss of Brønsted Acidity by Dehydroxylation and Dealumination. *J. Phys. Chem.* **1993**, *9*, 440−445.

(42) Su, B. L.; Lamy, A.; Dzwigaj, S.; Briend, M.; Barthomeuf, D. Oxidizing and Reducing Properties of SAPO-37 Molecular Sieve: Comparison with Acidity and Catalysis. *Appl. Catal.* **1991**, *75*, 311−320.

(43) Xu, T.; Munson, E. J.; Haw, J. F. Toward a Systematic Chemistry of Organic-Reactions in Zeolites—In-Situ NMR-Studies of Ketones. *J. Am. Chem. Soc.* **1994**, *116*, 1962−1972.

(44) Fang, H. J.; Zheng, A. M.; Chu, Y. Y.; Deng, F. C-13 Chemical Shift of Adsorbed Acetone for Measuring the Acid Strength of Solid Acids: A Theoretical Calculation Study. *J. Phys. Chem. C* **2010**, *114*, 12711−12718.

(45) Li, S. H.; Huang, J.; Shen, W. L.; Zhang, H. L.; Fang, H. J.; Zheng, A. M.; Liu, S. B.; Deng, F. Probing the Spatial Proximities among Acid Sites in Dealuminated H-Y Zeolite by Solid-State NMR Spectroscopy. *J. Phys. Chem. C* **2008**, *112*, 14486−14494.

(46) Jiang, Y. J.; Huang, J.; Dai, W. L.; Hunger, M. Solid-State Nuclear Magnetic Resonance Investigations of the Nature, Property, and Activity of Acid Sites on Solid Catalysts. *Solid State Nucl. Magn. Reson.* **2011**, *39*, 116−141.

(47) Martins, G. A. V.; Berlier, G.; Coluccia, S.; Pastore, H. O.; Superti, G. B.; Marchese, L. Revisiting the Nature of the Acidity in Chabazite-Related Silicoaluminophosphates: Combined FTIR and ^{29}Si MAS NMR Study. *J. Phys. Chem. C* **2007**, *111*, 330−339.

(48) Jeon, H. Y.; Shin, C. H.; Jung, H. J.; Hong, S. B. Catalytic Evaluation of Small-Pore Molecular Sieves with Different Framework Topologies for the Synthesis of Methylamines. *Appl. Catal., A* **2006**, *305*, 70−78.